AIP | Journal of Applied Physics

Tunneling current calculations for nonuniform and asymmetric multiple quantum well structures

Kasturi Mukherjee and N. R. Das

Citation: J. Appl. Phys. **109**, 053708 (2011); doi: 10.1063/1.3553391
View online: http://dx.doi.org/10.1063/1.3553391
View Table of Contents: http://jap.aip.org/resource/1/JAPIAU/v109/i5
Published by the American Institute of Physics.

Tunneling current calculations for nonuniform and asymmetric multiple quantum well structures

Kasturi Mukherjee[a] and N. R. Das[a]
Institute of Radio Physics and Electronics, University of Calcutta, 92 Acharya P. C. Road, Kolkata-700009, India

(Received 13 August 2010; accepted 24 December 2010; published online 9 March 2011)

In this paper, we present our studies on current-voltage characteristics due to tunneling in nonuniform and asymmetric multiple quantum well (MQW) structures. First, the transmission coefficient is calculated by solving the Schrödinger equation with the piecewise-constant potential approximation and by considering the effects of nonuniformity and the asymmetry of layer dimensions and band-offsets. Then the tunneling current through the structure is calculated as a function of bias for different structural combinations of the MQW structure. The configurations suitable for some applications are indicated in the results. © *2011 American Institute of Physics*. [doi:10.1063/1.3553391]

I. INTRODUCTION

Nanostructured devices have received a great deal of attention from researchers because of their ultra-small dimensions and improved functionality.[1] The tunability of the effective bandgap by energy quantization gives rise to novel electronic and optoelectronic properties.[2,3] Many such quantum effect devices are already commercially available. Multiple quantum well (MQW) structures have been used in making functional devices such as resonant tunneling diodes (RTD) and resonant tunneling transistors (RTT), quantum cascade lasers (QCL), quantum well infrared photodetectors (QWIP), quantum confined Stark effect modulators, etc. QCLs are preferred for broadband tuning,[4–6] RTD and RTT for multivalued digital logic and negative resistance devices,[7,8] QWIP for night vision, noninvasive medical diagnosis, environmental pollution monitoring,[9–14] etc. Tunneling in finite superlattices, high field domain formation in superlattices, and sequential resonant tunneling phenomena in multi-quantum well superlattices have already been investigated.[15–17] The importance of the use of an InGaAs/GaAs superlattice-based structure for an InGaP/GaAs superlattice-emitter bipolar transistor to satisfy the requirement of low turn on voltage and power consumption has recently been studied.[18] The necessity of incorporating a superlattice to act as an electron blocking layer to achieve temperature stable characteristics of an InGaN blue LED is made clear.[19] A reduction of the dark current in QWIP is one of the challenging tasks and thus the impact of barrier height, i.e., device geometry and doping concentration on the performance of QWIP is studied.[20] Therefore, MQWs have recently been a topic of immense interest to researchers, with the objective to search for new materials and designs for the best performance of MQW based devices. The areas of interest include tailoring the effective bandgap and energy state positions to achieve a low turn-on voltage for circuit applications, blocking of electrons for the temperature stable characteristics of optoelectronic devices, and enhancing the photocurrent to dark current ratio in QWIPs and many other applications. Most of the previous studies were based on the symmetric and uniform MQW structures. In some cases, it has been seen that asymmetry may improve the performance of MQW based devices. The enhanced slope efficiency of electro-absorption modulators,[21] high electric-field-sensitivity electro-absorption,[22] and photoluminescence in the deep ultraviolet region[23] can be realized using asymmetric quantum wells.

In this paper, we investigate theoretically the effect of asymmetry and nonuniformity of the layer thicknesses and potential barriers on the transmission coefficient and current transport properties of MQW structures. The sections are organized as follows. The transmission coefficient and current density are calculated in Sec. II. In Sec. III, results obtained from the computation are discussed. Finally, a conclusion is given in Sec. IV.

II. THEORY

We consider the conduction band diagram of a multiple quantum well structure shown in Fig. 1(a). The barrier and well layers are assumed to be undoped. One of the contact regions is serving as an emitter and the other as a collector. The collector is biased at positive voltage with respect to the emitter, the band bends downwards to the right, and electrons tunnel through barriers from the emitter to the collector resulting in the current through the structure [Fig. 1(b)]. The energy states in the quantum wells descend due to a potential drop across the layers of the MQW structure. Tunneling is determined by the penetration of the wave functions of electrons through the barriers. To calculate the energy states and electron transmission probability through the barriers, we need to solve the time-independent Schrödinger equation for each layer of the MQW structure. For example, the Schrödinger equation for region II (the leftmost barrier) under the biased condition is given by,

[a]Authors to whom correspondence should be addressed. Electronic addresses: kaskedar.mk@gmail.com and nrd@ieee.org.

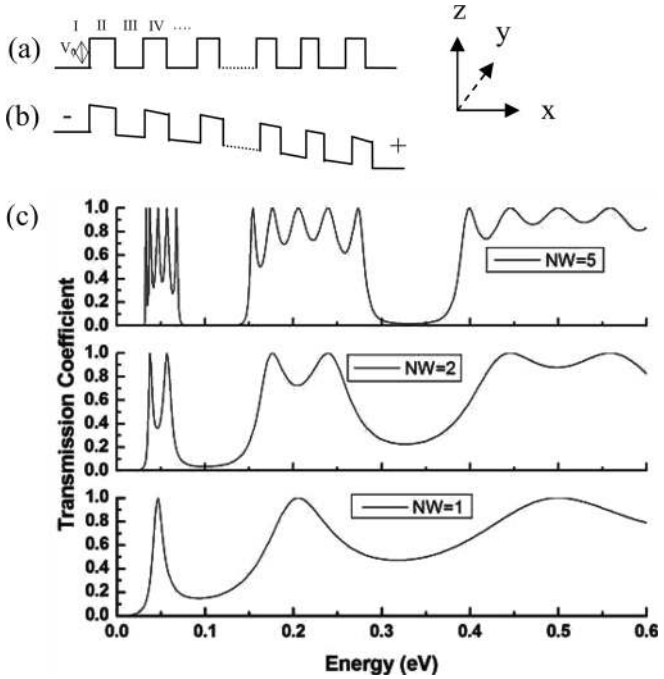

FIG. 1. (a) Conduction band (CB) diagram of an unbiased uniform MQW structure (e.g., $Al_{0.5}Ga_{0.5}As/GaAs$ has a CB offset of 0.5 eV), (b) biased MQW structure, (c) transmission coefficient vs energy of the uniform MQW structure with the number of wells (NW) as a parameter. The barrier width is fixed (0.8 nm), the well width is fixed (8 nm), and the barrier height is fixed (0.5 eV).

$$-\frac{\hbar^2}{2m^*}\frac{d^2\psi}{dx^2}+[V_0-e\varepsilon_1 L_1-e\varepsilon_2(x-L_1)]\psi(x)=E\psi(x), \quad (1)$$

where, $\hbar$ is the Dirac's constant, m^* is the effective mass of electrons, $\psi(x)$ is the wave function of electrons, V_0 is the barrier potential of the unbiased structure, e is the electronic charge, ε_i is the electric field in the ith region, L_i is the x-axis coordinate of the interface between the ith and $(i+1)$th region and E is the total energy. In the y-z plane, the electron motion is free. The general solution of Eq. (1) gives the wave function in a layer (e.g., the ith layer) under an electric field as follows,

$$\psi_i(x)=CAi(-\zeta_i)+DBi(-\zeta_i), \quad (2)$$

and

$$\varsigma_i=\left(2m^*e\varepsilon_i/\hbar^2\right)^{1/3}(x+E/e\varepsilon_i), \quad (3)$$

where Ai and Bi are Airy functions,[24] C and D are constants. Applying the boundary conditions (continuity of ψ and $\frac{1}{m^*}\frac{d\psi}{dx}$) at the interfaces, we can relate the wave functions in the neighboring regions by the propagation matrix ($\hat{P}$).[25]

$$\hat{P}=\begin{bmatrix} e^{ik_1L_1} & e^{-ik_1L_1} \\ e^{ik_1L_1} & -e^{-ik_1L_1}\end{bmatrix}^{-1}\begin{bmatrix} Ai(-\varsigma_2)_{L_1} & Bi(-\varsigma_2)_{L_1} \\ -\frac{a_2}{ik_1}Ai'(-\varsigma_2)_{L_1} & -\frac{a_2}{ik_1}Bi'(-\varsigma_2)_{L_1}\end{bmatrix}$$
$$\cdots\begin{bmatrix} Ai(-\varsigma_{n-1})_{L_{n-1}} & Bi(-\varsigma_{n-1})_{L_{n-1}} \\ Ai'(-\varsigma_{n-1})_{L_{n-1}} & Bi'(-\varsigma_{n-1})_{L_{n-1}}\end{bmatrix}^{-1}$$
$$\times\begin{bmatrix} e^{ik_nL_{n-1}} & e^{-ik_nL_{n-1}} \\ -\frac{ik_n}{a_{n-1}}e^{ik_nL_{n-1}} & \frac{ik_n}{a_{n-1}}e^{-ik_nL_{n-1}}\end{bmatrix} \quad (4)$$

and

$$a_i=\left(\frac{2m^*e\varepsilon_i}{\hbar^2}\right)^{1/3}, \quad (5)$$

where k_i is the wave vector in the ith region. The final propagation matrix in Eq. (4) relating the coefficients of the wave functions in the leftmost and the rightmost regions of the whole MQW structure is used to calculate the transmission coefficient ($\Im$) using the relation,

$$\Im=\frac{1}{|P_{11}|^2}, \quad (6)$$

The current density due to electrons incident from the left (J_L) is determined by the Fermi-Dirac distribution function and transmission coefficient.[15,25]

$$J_L=e\int_0^\infty\frac{dk_x}{2\pi}\frac{\hbar k_x}{m^*}\Im(k_x)\left[2\int\frac{d^2\vec{k}}{(2\pi)^2}f\left(E_{CL}+\frac{\hbar^2k_x^2}{2m^*}+\frac{\hbar^2k_s^2}{2m^*},E_{FL}\right)\right] \quad (7)$$

and

$$E(\vec{k})=E_{CL}+\frac{\hbar^2k_x^2}{2m^*}+\frac{\hbar^2k_s^2}{2m^*} \quad (8)$$

where, E_{CL} is the bottom of the conduction band on the left side, k_s is the wave vector in the y-z plane, E_{FL} is the Fermi energy on the left side, $v_x(\vec{k})$ is the velocity factor $(\hbar k_x/m^*)$ along the direction of electron tunneling. We can also similarly calculate the current density due to the electrons arriving from the right (J_R). The net current density (J) in the device is the algebraic sum of the current due to electrons impinging on the barrier from the left and right directions.

$$J=e\int_0^\infty\frac{dk_x}{2\pi}\frac{\hbar k_x}{m^*}\Im(k_x)n_{2D}\left(E_{FL}-E_{CL}-\frac{\hbar^2k_x^2}{2m^*}\right)$$
$$-e\int_0^\infty\frac{dk_x}{2\pi}\frac{\hbar k_x}{m^*}\Im(k_x)\left[n_{2D}\left(E_{FR}-E_{CR}-\frac{\hbar^2k_x^2}{2m^*}\right)\right], \quad (9)$$

where, E_{FR} and E_{CR} are the Fermi energy and the bottom of the conduction band in the right contact region, respectively. The component of energy due to motion along the x-direction is

$$E=E_C+\frac{\hbar^2k_x^2}{2m^*}, \quad (10)$$

Now, the density of electrons in a subband (n_{2D}) is given by

$$n_{2D}(E_F-E)=\frac{m^*k_BT}{\pi\hbar^2}\ln\left[1+\exp\left(\frac{E_F-E}{k_BT}\right)\right], \quad (11)$$

where k_B is the Boltzmann's constant, T is the temperature, and E_F is the Fermi energy. After mathematical simplifications Eq. (9) becomes

$$J = \frac{e}{h}\int_{E_{CL}}^{\infty} [n_{2D}(E_{FL} - E) - n_{2D}(E_{FR} - E)]\Im(E)dE \quad (12)$$

In a practical situation, up to Fermi energy all the levels are filled by electrons. So, the upper limit of the integration in Eq. (12) needs to be changed accordingly for numerical computation. The above equation shows that the tunneling current depends on the transmission coefficient, which again depends on the relative position of the subbands in neighboring wells of the multiple quantum well structure. The transmission coefficient is based on the accurate method of calculation using the propagation matrix approach. Thus, Eq.(12) gives the accurate nature of the tunneling currents.

A simplified form of Eq. (4) is obtained first by dividing each layer into a large number of segments and then assuming the piecewise-constant potential in different segments. This method had also been adopted earlier by other authors.[26] In our analysis, the increment in length is made very small, so the error due to discretization is very small. The boundary conditions are applied at the interfaces between the different segments. After several steps of calculation, we arrive at the following expression for the propagation matrix:

$$\begin{aligned}\hat{P} = &\begin{bmatrix} e^{ik_1L_1} & e^{-ik_1L_1} \\ e^{ik_1L_1} & -e^{-ik_1L_1} \end{bmatrix}^{-1} \begin{bmatrix} e^{ik_{21}L_1} & e^{-ik_{21}L_1} \\ \frac{k_{21}}{k_{1,m}}e^{ik_{21}L_1} & -\frac{k_{21}}{k_{1,m}}e^{-ik_{21}L_1} \end{bmatrix} \\ &\times \begin{bmatrix} e^{ik_{21}(L_1+d)} & e^{-ik_{21}(L_1+d)} \\ e^{ik_{21}(L_1+d)} & -e^{-ik_{21}(L_1+d)} \end{bmatrix}^{-1} \begin{bmatrix} e^{ik_{22}(L_1+d)} & e^{-ik_{22}(L_1+d)} \\ \frac{k_{22}}{k_{21}}e^{ik_{22}(L_1+d)} & -\frac{k_{22}}{k_{21}}e^{-ik_{22}(L_1+d)} \end{bmatrix} \cdots \\ &\times \begin{bmatrix} e^{ik_{n-1,m}L_{n-1}} & e^{-ik_{n-1,m}L_{n-1}} \\ e^{ik_{n-1,m}L_{n-1}} & -e^{-ik_{n-1,m}L_{n-1}} \end{bmatrix}^{-1} \begin{bmatrix} e^{ik_nL_{n-1}} & e^{-ik_nL_{n-1}} \\ \frac{k_{n,1}}{k_{n-1,m}}e^{ik_nL_{n-1}} & -\frac{k_{n.,1}}{k_{n-1,m}}e^{-ik_nL_{n-1}} \end{bmatrix}\end{aligned} \quad (13)$$

where d is the length of each sub-region and k_{ij} represents the wave vector of the jth sub-region of the ith region given by

$$k_{ij} = \sqrt{\frac{2m_i^*(E - V_{ij})}{\hbar^2}}, \quad (14)$$

where m_i^* is the effective mass of the electron in the ith region and $V_{ij,}$ the potential of the jth sub-region of the ith region. The above propagation matrix is used to calculate the transmission coefficient and current density using the formulas mentioned earlier.

III. RESULTS AND DISCUSSION

Using Eq. (6), the transmission coefficient is computed and plotted versus energy for single well, double well, and five well structures as shown in Fig. 1(c). The peak in the transmission coefficient for a single well structure indicates resonant transmission, when the incident energy aligns with an energy state in the well. Sharp peaks indicate the presence of discrete states in the well. For two-well structures, two close peaks at the low energy position indicate the splitting of the lowest energy state due to the interaction between the two wells. When the number of wells is five, more closely spaced peaks are found in the lowest energy position. Thus, as the number of wells increases, spacing between the split energy states decreases to form a quasicontinuous miniband. The miniband formed from the coupled higher excited state spreads over a broader energy range [Fig. 1(c)].

However, the coupling between the wells depends on the barrier width separating the wells in the MQW structure. The effect of the barrier-to-well width (B/W) ratio on the transmission coefficient is shown in Fig. 2. In all cases, the well width is kept constant. In this paper, the current density is converted to a dimensionless quantity by dividing it with $(em^*(k_BT)^2/2\pi^2\hbar^3)$. It can be seen that as the barrier-to-well width ratio increases, the spread of the miniband shrinks, and the separation of the miniband increases [Fig. 2(a)]. For a large barrier-to-well width ratio the miniband turns to a single sharp transmission peak [Fig. 2(a)]. The variation of spread in miniband as a function of B/W ratio is shown in Fig. 2(b). It can be seen that the spread decreases with an increase in the B/W ratio. Additionally the spread of the higher miniband increases more rapidly than in the ground state as the B/W ratio decreases. In the following paragraphs, we study the effects of structural nonuniformity and asymmetry on the current-voltage characteristics of multiple quantum well structures. As similar experimental studies are not found in the literature, we have compared our model with experimental data on a single-well double-barrier structure reported in Ref. 27 where the structure has a 5 nm well width, an 8 nm barrier width and a 0.4 eV barrier height. The experimental results[27] show the first two current peaks for positive bias at $\sim$0.19 and $\sim$0.79 V. Using our model for the similar structure, the corresponding peaks are obtained at 0.2 and 0.75 V. Thus, the model results are in good agreement with the experimental data.

The effect of barrier -to- well width ratio on the current density versus voltage characteristics of a uniform and symmetric five-well structure is shown in Fig. 3. In parts (i), (ii), and (iii) of the figure, the results are shown for different barrier-to-well width ratios. The conduction band gets tilted and the energy levels decrease due to the applied bias so the relative position of the energy levels in the adjacent quantum wells changes. An appropriate bias can align the ground state of one well with the excited state of the next well and resonant tunneling is also possible in this case. The miniband starts at a lower energy for a smaller barrier-to-well width

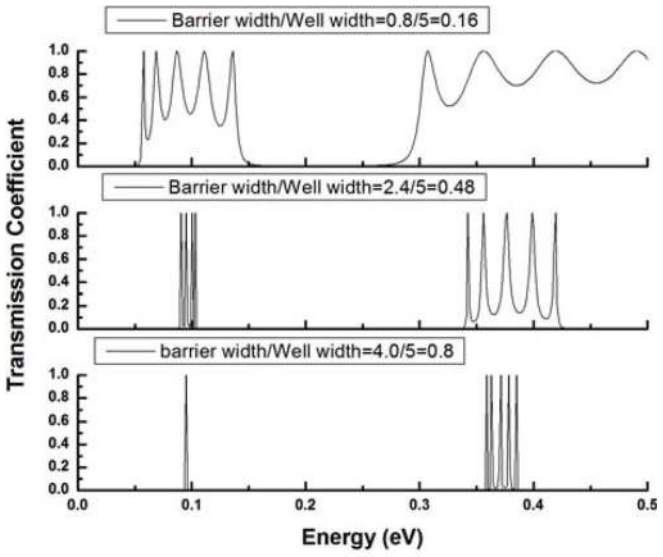

(a)

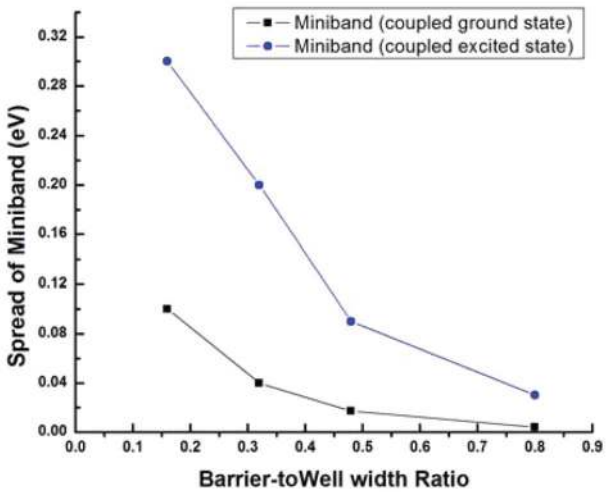

(b)

FIG. 2. (Color online) (a) Transmission coefficient vs energy plot of uniform MQW structure (number of wells = 5) with the barrier-to-well width ratio (B/W) as a parameter. The well width is fixed (5 nm) and the barrier height is fixed (0.5 eV). (b) Spread of the miniband vs barrier-to-well width ratio of the uniform MQW structure (number of wells = 5). The barrier height is fixed (0.5 eV).

ratio. So, the tunneling current is available at a lower bias. With the increase in barrier-to-well width ratio, the current density at low bias becomes quantized with consequent improvement in the peak-to-valley ratio. However, the quantized current at low bias disappears when the B/W ratio is large [Fig. 3(iii)]. This quantized conduction is useful for implementing filtering or switching action.

Now we investigate the effect of nonuniformity or asymmetry of layer thicknesses and barrier heights on the current-voltage characteristics of the MQW structures. Here, we consider nonuniform but symmetric MQW structures of different well widths keeping the barrier widths and heights constant [Fig. 4]. The results are shown for the well width increasing outward and for the well width decreasing outward slowly from the center. In the nonuniform structure with the well width increasing outward from the center well,

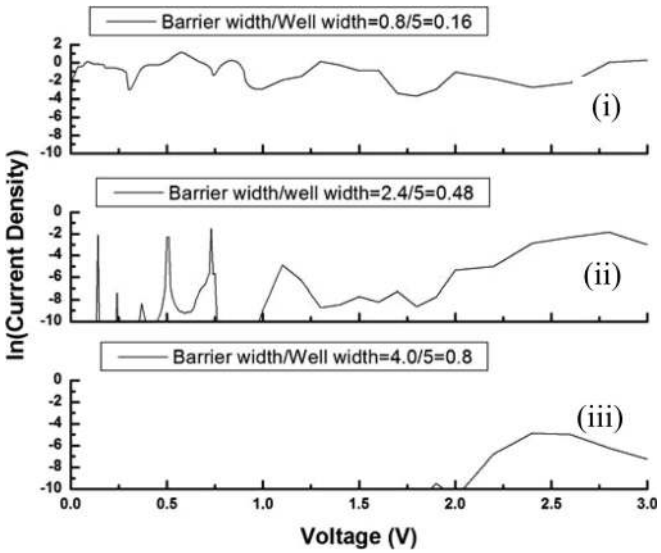

FIG. 3. Current density vs voltage plot of uniform MQW structure (number. of wells = 5) with the barrier-to-well width (B/W) ratio (i) 0.16, (ii) 0.48, and (iii) 0.8. The well width is fixed(5 nm) and the barrier height is fixed(0.5 eV).

energy levels at the outer wells are positioned at a lower energy compared to the middle well. Thus current conduction initiates at lower bias [Figs. 4(ii) and 4(iii)] than uniform structure [Fig. 4(i)]. The structure with well width decreasing outward and energy levels lying at higher energy near contact ends, [Figs. 4(iv) and 4(v)] shows conduction initiates at a larger bias. Magnitudes of different peaks differ due to the variation of the electron transmission coefficient at different biases. The current density peaks at the lowest voltage results from the alignment of the ground state of one well with the ground state of the neighboring well. In another situation, when the ground state of one well is aligned with the

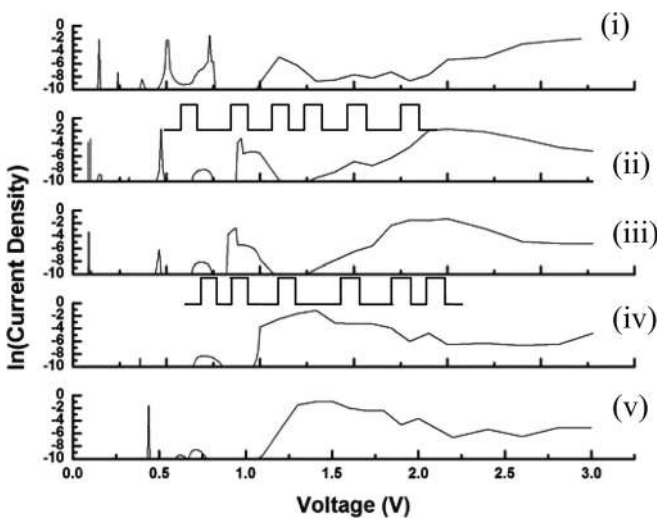

FIG. 4. Current density vs voltage for MQW structure (number of wells = 5) with (i) uniform structure (barrier width = 2.4 nm, well width = 5 nm, and barrier height = 0.5 eV), (ii) well widths increasing outward from the center (values = 6, 5.5, 5, 5.5, and 6 nm), (iii) well widths increasing outward from the center (values = 6.4, 5.7, 5, 5.7, and 6.4 nm), (iv) well widths decreasing outward from the center (values = 3, 4, 5, 4, and 3 nm), (v) well widths decreasing outward from the center (values = 2.6, 3.8, 5, 3.8, and 2.6 nm). In each case, the barrier width is fixed (2.4 nm) and the barrier height is fixed (0.5 eV).

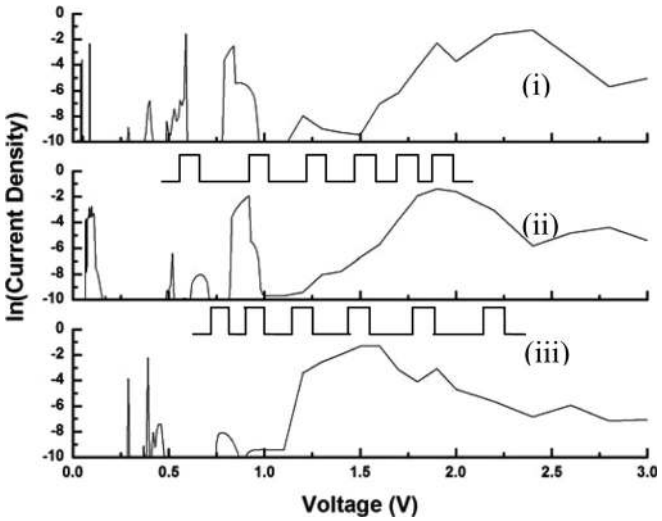

FIG. 5. Current density vs voltage for MQW structure (number of wells = 5) with (i) uniform structure (barrier width = 2.4 nm, well width = 6 nm, and barrier height = 0.5 eV), (ii) well width decreasing toward the right (values = 6, 5.5, 5, 4.5, and 4 nm), (iii) well widths increasing toward the right side (values = 3, 4, 5, 6, and 7 nm). In each case, the barrier width is fixed (2.4 nm) and the barrier height is fixed (0.5 eV).

higher state of the adjacent well, then the current also starts to conduct at low bias.

The results for asymmetric MQW structures are shown in Fig. 5. The current-voltage characteristics of the structure with well widths decreasing toward the right contact [Fig. 5(ii)] yields a quantized current band at a slightly lower bias compared to the symmetric structure [Fig. 5(i)]. However, current conduction initiates at a relatively higher bias in the asymmetric structure with well widths increasing toward the right (collector end) [Fig. 5(iii)]. Both types of asymmetry shows an early onset of continuous current.

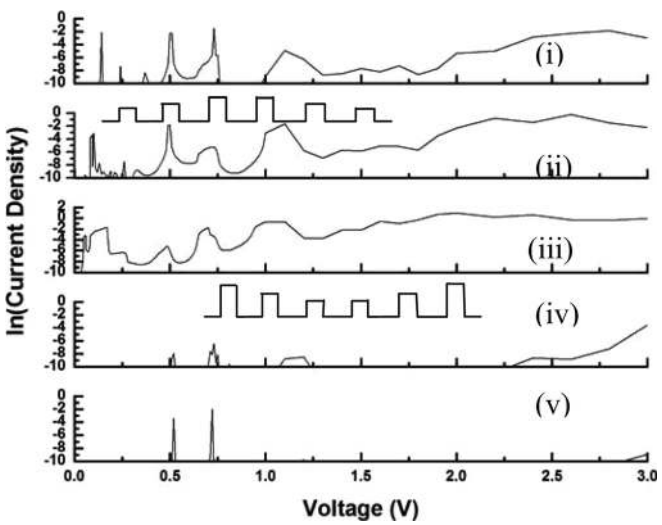

FIG. 6. Current density vs voltage for MQW structure (number of wells = 5) with (i) uniform structure (barrier width = 2.4 nm, well width = 5 nm, and barrier height = 0.5 eV), (ii) barrier heights decreasing outward from the center (values = 0.3, 0.4, 0.5, 0.5, 0.4, and 0.3 eV), (iii) barrier heights decreasing outward from the center (values = 0.1, 0.3, 0.5, 0.5, 0.3, and 0.1 eV), (iv) barrier heights increasing outward from the center (values = 0.9, 0.7, 0.5, 0.5, 0.7, and 0.9 eV), (v) barrier heights increasing outward from the center (values = 1.1, 0.8, 0.5, 0.5, 0.8, and 1.1 eV). In each case, the barrier width is fixed (2.4 nm) and the well width is fixed (5 nm).

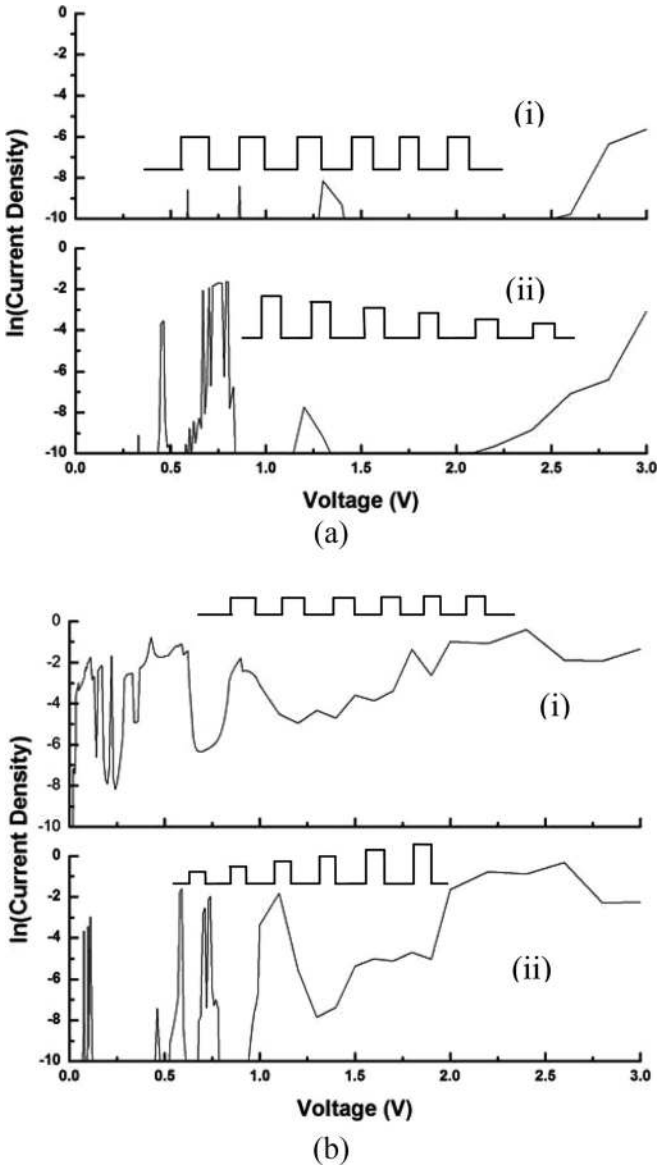

FIG. 7. Current density vs voltage for MQW structure (number of wells = 5) with (a) (i) uniform structure (barrier width = 2.4 nm, well width = 5 nm, and barrier height = 0.8 eV), (a) (ii) barrier heights decreasing toward the right side (values = 0.8, 0.7, 0.6, 0.5, 0.4, and 0.3 eV), (b) (i) uniform structure (barrier width = 2.4 nm, well width = 5 nm, and barrier height = 0.3 eV), (b) (ii) barrier heights increasing toward the right side (values = 0.3, 0.4, 0.5, 0.6, 0.7, and 0.8 eV). In each case, the barrier width is fixed (2.4 nm) and the well width is fixed (5 nm).

The effect of barrier height variation on the current versus voltage characteristics of the nonuniform but symmetric MQW structure is shown in Fig. 6. The structure with the barrier height decreasing outward from the center [Figs. 6(ii) and (iii)] supports the continuous current transport starting at a lower bias than in the case of the uniform structure [Fig. 6(i)]. The current-voltage characteristics of the MQW structure with the barrier height increasing outward from the center [Figs. 6(iv) and (v)] shows the onset of current conduction at higher biases. The smaller the difference is between successive barrier heights [Fig. 6(iv)], the better the blocking of current flow is for a wide range of voltages. Thus this type of structure may help in reducing the dark current of a MQW intersubband photodetector.

We investigate the current density versus voltage characteristics of another type of asymmetric MQW structure with variable barrier heights in Fig. 7. The structure with the barrier heights decreasing from the emitter end to the collector end [Fig. 7(a)(ii)], displays the current band at a lower voltage compared to the symmetric structure [Fig. 7(a)(i)]. The structure with barrier heights increasing from left to right, [Fig. 7(b)(ii)], shifts initiation of the current transport to higher voltages compared to that in Fig. 7(b)(i). Hence, the MQW structure with a small conduction band offset can exhibit quantized conduction characteristics when it is asymmetric in dimension.

IV. CONCLUSION

The miniband formed due to the coupling of ground states in neighboring wells spreads over a narrower energy range than due to the coupling between the higher states. The spread of the minibands decreases and the spacing between two minibands increases as the barrier-to-well width ratio is increased. The nonuniform MQW structure with well widths increasing outward from the center well provides a low turn-on voltage for current transport compared to the symmetric structure. If the ground state of one well is resonant with the higher state of the adjacent well, then first current peaks can also be seen at low bias. This type of structure can be used for a low-power electronic switch in circuit applications. The nonuniform structure with barrier heights increasing outward from the center yields a very small magnitude of current density at a relatively larger bias. Even a continuous current of an insignificant magnitude begins to flow at larger bias. Hence, the MQW structure with barrier heights increasing outward from the center is suitable for blocking current conduction over low bias ranges. This structure is thus preferable to keep the dark current low over a wide range of applied positive voltages in quantum well intersubband photodetectors. This study focuses on how the tunneling current depends on the choice of different kinds of structural nonuniformity and asymmetry of the multiple quantum well structure using only undoped layers. The presence of doped layers may perturb the potential profile, thus affecting the transmission coefficient and hence the tunneling current. Therefore, to deal with a more generalized situation, the structures with doped layers should be considered.

ACKNOWLEDGMENTS

The work is financially supported by the Council of Scientific & Industrial Research (CSIR), India under the Senior Research Fellowship scheme.

[1]K. Goser, P. Glosekotter, and J. Dienstuhl, *Nanoelectronics and Nanosystems: From Transistors to Molecular and Quantum Devices* (Springer, Berlin, 2004).
[2]S. Bhattacharyya, N. R. Das, and S. Sen, J. Appl. Phys. **105**, 053108 (2009).
[3]A. Bismuto, R. Terazzi, M. Beck, and J. Faist, Appl. Phys. Lett. **96**, 141105 (2010).
[4]A. Wittmann, T. Gresch, E. Gini, L. Hvozdara, N. Hoyler, and M. Giovannini, IEEE J. Quantum Electron. **44**, 36 (2008).
[5]Y. Yao, W. O. Charles, T. Tsai, J. Chen, G. Wysocki, and C. F. Gmachl, Appl. Phys. Lett. **96**, 211106 (2010).
[6]K. Fujita, T. Edamura, S. Furuta, and M. Yamanishi, Appl. Phys. Lett. **96**, 241107 (2010).
[7]L. Worschech, F. Hartmann, T. Y. Kim, S. Höfling, M. Kamp, A. Forchel, J. Ahopelto, I. Neri, A. Dari, and L. Gammaitoni, Appl. Phys. Lett. **96**, 042112 (2010).
[8]K. Hinata, M. Shiraishi, S. Suzuki, M. Asada, H. Sugiyama, and H. Yokoyama, Appl. Phys. Express. **3**, 014001 (2010).
[9]S. U. Eker, M. Kaldirim, Y. Arslan, and C. Besikci, IEEE Electron Device Lett. **29**, 1121 (2008).
[10]H. C. Liu, J. Appl. Phys. **73**, 3062 (1993).
[11]S. D. Gunapala, B. F. Levine, L. Pfeiffer, and K. West, J. Appl. Phys. **69**, 6517 (1991).
[12]E. Lhuillier, N. Pere-Laperne, I. Ribet-Mohamed, E. Rosencher, G. Patriarche, A. Buffaz, V. Berger, A. Nedelcu, and M. Carras, J. Appl. Phys. **107**, 123110 (2010).
[13]C. A. Kukkonen, M. N. Sirangelo, R. Chehayeb, M. Kaufmann, J. K. Liu, S. B. Rafol, and S. D. Gunapala, Infrared PhysTechnol. **42**, 397 (2001).
[14]H. Schneider, H. C. Liu, S. Winnerl, C. Y. Song, M. Walther, and M. Helm, Opt. Express **17**, 12279 (2009).
[15]R. Tsu and L. Esaki, Appl. Phys. Lett. **22**, 562 (1973).
[16]L. Esaki and L. L. Chang, Phys. Rev. Lett. **33**, 495 (1974).
[17]F. Capasso, K. Mohammed, and A. Y. Cho, Appl. Phys. Lett. **48**, 478 (1986).
[18]J. Tsai, Y. Lee, N. Dale, J. Sheng, Y. Ma, and S. Ye, Appl. Phys. Lett. **96**, 063505 (2010).
[19]K. S. Kim, J. H. Kim, S. J. Jung, Y. J. Park, and S. N. Cho, Appl. Phys. Lett. **96**, 091104 (2010).
[20]X. G. Guo, R. Zhang, H. C. Liu, A. J. SpringThorpe, and J. C. Cao, Appl. Phys. Lett. **97**, 021114 (2010).
[21]D. K. Kim and D. S. Citrin, IEEE J. Quantum Electron. **43**, 765 (2007).
[22]D. K. Kim and D. S. Citrin, IEEE J. Quantum Electron. **43**, 651 (2007).
[23]G. Sun, Y. J. Ding, G. Liu, G. S. Huang, H. Zhao, N. Tansu, and J. B. Khurgin, Appl. Phys. Lett. **97**, 021904 (2010).
[24]Handbook of Mathematical Functions, edited by M. A. Abramowitz and I. A. Stegun (Dover, New York, 1965).
[25]John H. Davies, *The Physics of Low-Dimensional Semiconductors: An Introduction* (Cambridge University Press, Cambridge, 1998).
[26]Y. Ando and T. Itoh, J. Appl. Phys. **61**, 1497 (1987).
[27]L. L. Chang, L. Esaki, and R. Tsu, Appl. Phys. Lett. **24**, 593 (1974).